The 2006 July 17 Java (Indonesia) tsunami from satellite imagery and numerical modelling: a single or complex source?

H. Hébert, P.-E. Burg, R. Binet, F. Lavigne, Sébastien Allgeyer, F. Schindelé

Geophysical Journal International

Geophys. J. Int. (2012) **191,** 1255–1271 doi: 10.1111/j.1365-246X.2012.05666.x

The 2006 July 17 Java (Indonesia) tsunami from satellite imagery and numerical modelling: a single or complex source?

H. Hébert,[1] P.-E. Burg,[1,2] R. Binet,[1] F. Lavigne,[2] S. Allgeyer[1] and F. Schindelé[1]

[1]*CEA, DAM, DIF,* 91297 *Arpajon, France. E-mail: helene.hebert@cea.fr*

[2]*Laboratoire de Géographie Physique, Université Paris* 1 *Panthéon-Sorbonne, UMR* 8591, 1 *Place Aristide Briand,* 92195 *Meudon Cedex, France*

Accepted 2012 September 3. Received 2012 September 3; in original form 2011 June 27

SUMMARY

The M_w 7.8 2006 July 17 earthquake off the southern coast of Java, Indonesia, has been responsible for a very large tsunami causing more than 700 casualties. The tsunami has been observed on at least 200 km of coastline in the region of Pangandaran (West Java), with run-up heights from 5 to more than 20 m. Such a large tsunami, with respect to the source magnitude, has been attributed to the slow character of the seismic rupture, defining the event as a so-called tsunami earthquake, but it has also been suggested that the largest run-up heights are actually the result of a second local landslide source. Here we test whether a single slow earthquake source can explain the tsunami run-up, using a combination of new detailed data in the region of the largest run-ups and comparison with modelled run-ups for a range of plausible earthquake source models.

Using high-resolution satellite imagery (SPOT 5 and Quickbird), the coastal impact of the tsunami is refined in the surroundings of the high-security Permisan prison on Nusa Kambangan island, where 20 m run-up had been recorded directly after the event. These data confirm the extreme inundation lengths close to the prison, and extend the area of maximum impact further along the Nusa Kambangan island (about 20 km of shoreline), where inundation lengths reach several hundreds of metres, suggesting run-up as high as 10–15 m.

Tsunami modelling has been conducted in detail for the high run-up Permisan area (Nusa Kambangan) and the PLTU power plant about 25 km eastwards, where run-up reached only 4–6 m and a video recording of the tsunami arrival is available. For the Permisan prison a high-resolution DEM was built from stereoscopic satellite imagery. The regular basin of the PLTU plant was designed using photographs and direct observations. For the earthquake's mechanism, both static (infinite) and finite (kinematic) ruptures are investigated using two published source models. The models account rather well for the sea level variation at PLTU, showing a better agreement in arrival times with the finite rupture, and predict the Permisan area to be one of the regions where tsunami waves would have focussed. However, the earthquake models that match the data at PTLU do not predict that the wave heights at Permisan are an overall maximum, and do not predict there more than 10 m of the 21 observed. Hence, our results confirm that an additional localized tsunami source off Nusa Kambangan island, such as a submarine landslide, may have increased the tsunami impact for the Permisan site. This reinforces the importance for hazard assessment of further mapping and understanding local potential for submarine sliding, as a tsunami source added to usual earthquake sources.

Key words: Tsunamis; Subduction zone processes; Submarine landslides; Indian Ocean.

1 THE 2006 JULY 17 EARTHQUAKE AND TSUNAMI

The 2006 July 17 earthquake occurred on the Java Trench (Fig. 1), about 200 km south to a coast where holiday resorts host thousands of tourists, especially in the Pangandaran area. The M_w magnitude estimated to 7.8, the thrusting mechanism and the shallow depth (almost 10 km) of the event were such that a tsunami was triggered, which reached the Java coastline within 1 hr following the main shock (Lavigne *et al.* 2007), and caused more than 700 casualties among harbours, holiday resorts and beaches.

1.1 A 'tsunami earthquake'

The very high tsunami heights (in excess of 10 m) rapidly reported in the devastated area were actually much larger than the moment

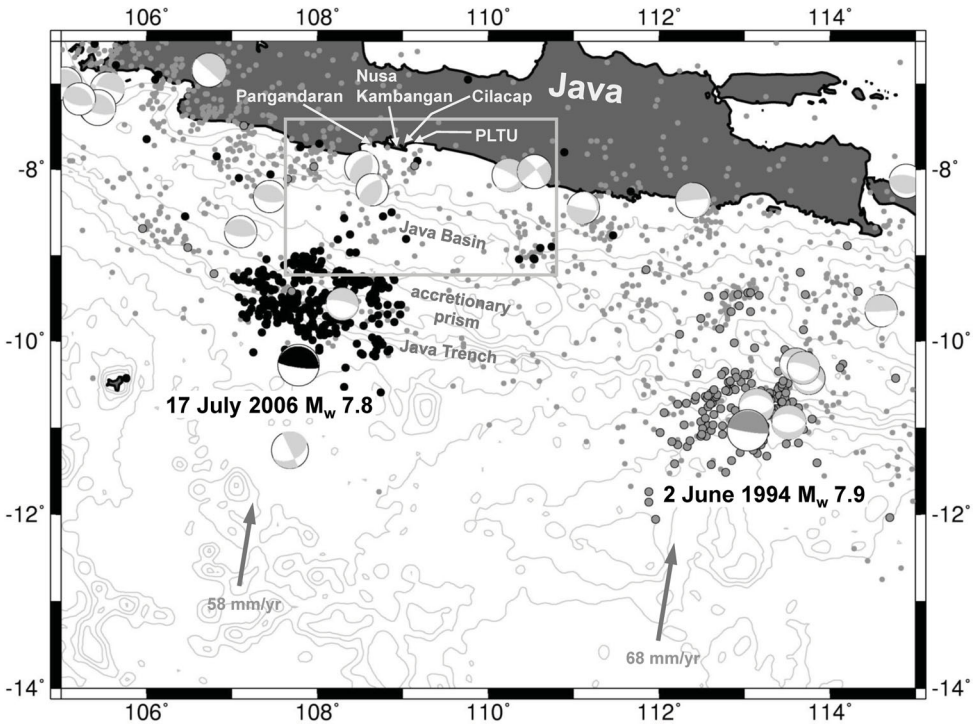

Figure 1. Context of the studied area south to Java Island. USGS seismicity since 1973 ($M > 4.5$) is shown with grey dots, while USGS aftershocks for the 2006 and 1994 earthquakes are shown with black and dark grey dots, respectively. Light grey focal mechanisms from CMT Harvard are displayed for $M_w > 6.0$, and main shocks CMT for the 2006 and 1994 events are shown in black and dark grey, respectively. Arrows denote the convergence of the Australia plate with respect to the Sunda plate (from Bird 2003). The rectangular area describes the extent of the first subgrid used for tsunami modelling.

magnitude of the event could have indicated, suggesting that the earthquake was a so-called 'tsunami earthquake' (Kanamori 1972). The 2006 earthquake occurred about 500 km to the west of a former strong earthquake that struck eastern Java in 1994 ($M_w = 7.9$), and that similarly had triggered an important tsunami (Maramai & Tinti 1997; Abercrombie *et al.* 2001). This earlier event was also recognized as a 'tsunami earthquake': the earthquake rupture was very shallow, thus possibly involving the thick sedimentary layers in the accretionary wedge, combined to a very heterogeneous subducting plate, all these characteristics contributing to variations in frictional properties during the rupture (Polet & Thio 2003). Most of these events create huge tsunami waves regarding their magnitude, which rarely exceed 7.5–7.9. Their rupture is assumed to be slow, as it was also suggested for the 2006 earthquake, reflecting several sequences of moment release on a smooth rupture consistent with a surrounding weak material (Ammon *et al.* 2006).

As in 1994, or in 1992 in Nicaragua (Satake 1994), or in 1996 in Peru (Heinrich *et al.* 1998), these events were found to be unusually rich in low-frequency energy released at shallow depths below the seafloor where it is especially efficient in triggering tsunami waves. These seismic events, usually hardly felt by coastal populations because of their moderate high-frequency waves, pose a great danger regarding the tsunami hazard since the common warning produced by the seismic shaking does not urge populations to escape on the surrounding heights. In addition Watch Bulletins issued in less than 20 min after the quake by Pacific Tsunami Warning Center and Japan Meteorological Agency (International Tsunami Information Center 2006) could not be efficiently delivered to local authorities (Mori *et al.* 2007).

1.2 Run-up data set

A series of several international survey teams dispatched to the affected area in the days and weeks following the tsunami. Most of them are summarized in Fig. 2. Within the first days, Japanese and Indonesian scientists revealed the extent of the impacted coastline, above 250 km in length (Mori *et al.* 2007), especially in the area of the Pangandaran tourist resorts. Severe damage (from collapsed walls to complete destruction) was reported within several hundreds of metres from the shore; consistent with run-up values from 6 to 8 m on average. The data collected by another Japanese team (Tsuji, http://www.eri.u-tokyo.ac.jp/tsunami/javasurvey/index_e.htm; PARI-JSCE Group, http://www.nda.ac.jp/~fujima/TMD/index.html) confirmed these values, both in longitudinal extent (at least 200 km) and amplitude (above 4–6 m), with an especially high value (6.2 m) close to the Power Plant PLTU (6 km NE to Cilacap), and the largest run-up (11.4 m) west of Pangandaran. A study of sedimentary deposits in the region of Cilacap also indicates a sandy layer up to 20 cm thick, that is consistent with the passage of at least two individual waves (Moore *et al.* 2011).

All these surveys had missed the extreme tsunami run-up values gathered when the Nusa Kambangan island was finally reached by two different teams. This island, only separated from Java by a narrow channel, hosts a high security prison close to the city of Permisan, and access is therefore very restricted. Extreme run-up values were measured here, up to 21- and 10-m-high water waves inundated the wide place cleared in the tropical forest where the prison is built (Fritz *et al.* 2007). Another team also confirmed very

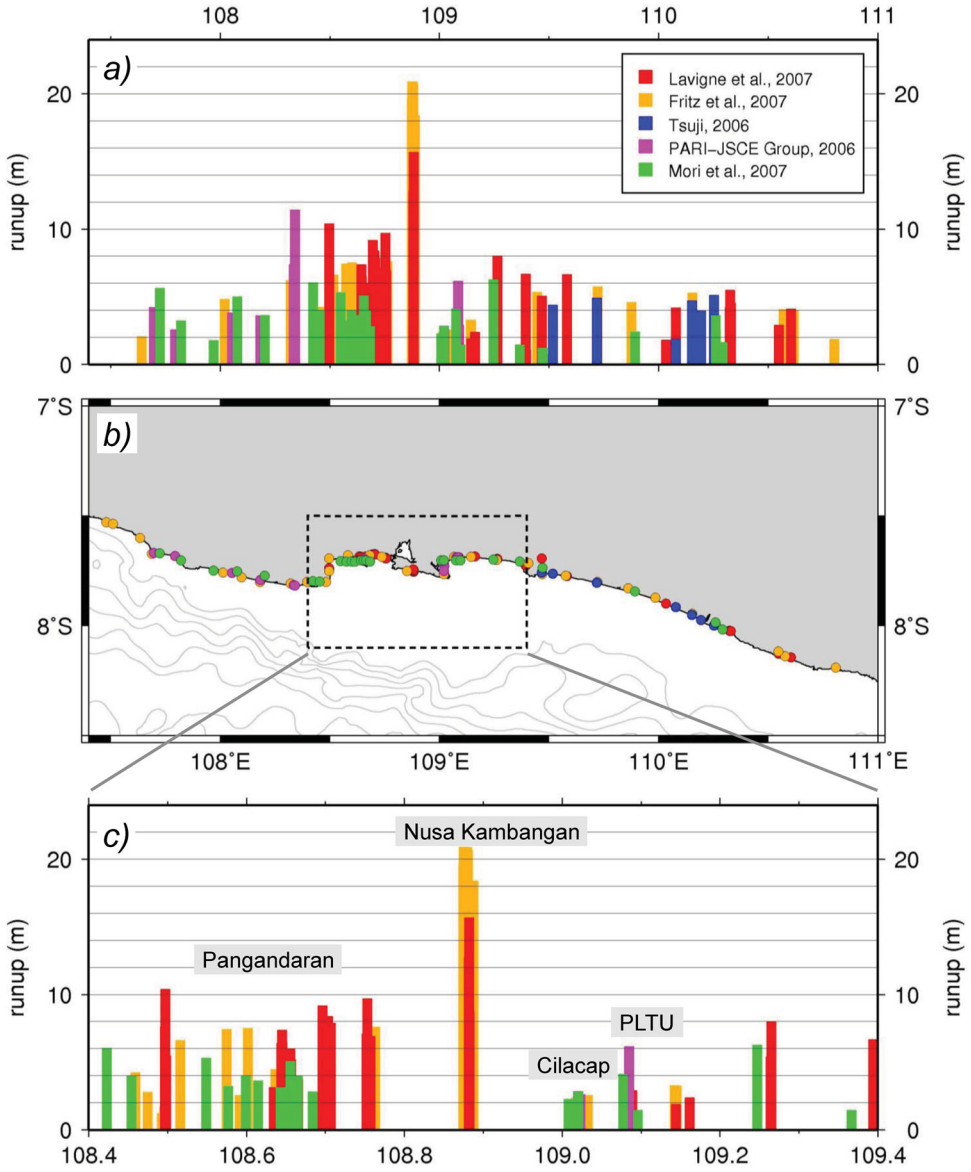

Figure 2. Synthesis of run-up observations gathered along the South Java coastline, for various survey teams. Only values identified as run-up have been plotted (a) along the coastline from 107.4°E to 111°E, (b) on the corresponding geographic map (with dashed rectangular area showing the computational grid 2) and (c) on the region around Nusa Kambangan island where maximum values have been reported (from PARI-JSCE Group 2006; Tsuji 2006; Fritz *et al.* 2007; Lavigne *et al.* 2007).

high flow depths and run-up heights of 15.7 m (Lavigne *et al.* 2007) close to the prison.

1.3 Which kind of source for such a large tsunami?

The overall tsunami data set (Fig. 2) exhibits an average tsunami height of 4–8 m along 200 km at least, and the reported values in the Permisan area are strikingly exceeding this trend. This large tsunami impact questions the possibility for an additional source to have contributed to these high amplitudes, namely a submarine landsliding source, as is accepted for some events, as in Papua New Guinea in 1998 (Heinrich *et al.* 2001), and as was already suggested for this 2006 event. Indeed the very localized extreme 21 m run-up measured in the Permisan area was attributed to a possible contribution of an additional submarine landslide (Fritz *et al.* 2007). Such a landslide source generally contributes to extreme run-up values along a coastal portion less extended than for earthquake sources (Okal & Synolakis 2004), a pattern which besides provides a way to discriminate the tsunami origin.

In this purpose of investigating the relative importance of both possible sources, we first need a better assessment of the extent of the high run-up area along the coast. In the following study, we provide additional constraints given by a detailed analysis of satellite imagery in the area of maximum run-up values on the Nusa Kambangan island, confirming very large values reached all along this shoreline. Then, using available earthquake rupture parameters for the 2006 earthquake, we carry out for the first time detailed numerical modellings of the tsunami in the area of the Permisan prison, where the highest run-up height was reported (Fritz *et al.* 2007; Lavigne *et al.* 2007), and where we use satellite images to build a refined elevation model. We also model the tsunami for the PLTU power plant basin, located to the east of Cilacap City, where a surveillance camera recording has been converted into a temporal

sea level variation (Lavigne *et al.* 2007) and can be compared to models. Finally, on the basis of the imagery analysis and of the tsunami modelling, we discuss the source process that was responsible for this large tsunami, indicating that an additional landslide source may also be requested to better explain the observation for the Nusa Kambangan island specifically.

2 RUN-UP DISTRIBUTION FROM REMOTE SENSING DATA

In this section we attempt to complement the original data set using high-resolution satellite imagery. On a regional scale, we show that the whole coastline of the Nusa Kambangan island was struck by tsunami waves having reached inundation distances similar to the Permisan area.

2.1 Method

In the aftermath of strong tsunamis, satellite imagery is more and more frequently used to identify the devastated areas, provide guidance for the rescuing operations and help to characterize the event, especially in comparing with field survey data (Fritz *et al.* 2008, 2011). Space agencies support these activities while giving rapid access to high-resolution images in the days following such events, for instance in the frame of the International Charter Space and Major Disasters (International Charter 2011). Concerning tsunamis, they give additional constraints on the flooding extent, the damage intensity and the coastal vulnerability (Borrero 2005; Chen *et al.* 2006). Providing accurate run-up values is more difficult from these imagery data, since this requires to estimate the altitudes, which may be possible using a stereographic approach, with a couple of images, but high-resolution digital elevation models (DEMs) are rarely available in remote areas.

Here we aim at providing additional tsunami characteristics in the area of the Nusa Kambangan island, that encompasses the maximum tsunami impact in the Permisan area, using, first, SPOT images with a resolution from 20 m (SPOT2, multispectral) to 10 m (SPOT5, multispectral), and second, a Quickbird image with a resolution of 2.4 m (multispectral) and 0.6 m (panchromatic) for refined analyses. These images allow us to define the impacted areas on the Nusa Kambangan island. The image's processing involved orthorectification, coregistration and, for Quickbird images, pan-sharpening to combine panchromatic and multispectral contents, thus allowing a facilitated analysis. The coastline has been digitized from both SPOT or Quickbird sources.

2.2 Estimation of the impact on the Nusa Kambangan island

The SPOT2 image from 2006 June 26 was the only one available, acquired only a few weeks prior to the 2006 July 17 event, and is thus used as the pre-event reference for this study. With a 60×60 km^2 spatial extent and a 20 m resolution, it offers a regional view of the Java coast near Pangandaran, which can be easily studied through the near infrared channel (Fig. 3, top panel). The post-event SPOT5 image from 2006 July 22 has a 10 m resolution in near-infrared, and does not cover the easternmost extremity of the island as did the SPOT2 image (Fig. 3, centre). However the Quickbird images from 2006 November 14 and 27 partly overcome this missing zone (Fig. 3, bottom panel).

The SPOT5 image allows defining four areas impacted by the tsunami between 108°48′E and 108°52′E (Fig. 4). The pre-event image does not reveal any cleared areas close to the coast, even near 108°49′E where the cloud cover seems more important and could be interpreted as a plough or bare soil. However the post-event image clearly exhibits four coastal areas where the vegetation has been cleared, and where the soil is bare (marked in green in Fig. 4, bottom panel), each of these places corresponding to small bays, and probably to river mouths. The horizontal distance from the shore to the forest border ranges from 100 to 300 m. Near 108°52′E, the impact seems to be more limited since the forest is only partially cleared and several trees remain. This kind of impact has been marked in blue in Fig. 4.

Further east, near 108°54′E, the pre-event SPOT2 image reveals probable old cultivated fields, or at least cleared areas, that may have facilitated tsunami waves to penetrate (Fig. 5). The post-event SPOT5 image shows an almost rectangular, NS elongated area with a horizontal distance from the shore reaching 500 m, again corresponding to a bay, and clearly exhibiting a river mouth. The pre-event cleared forest is enhanced in the post-event image, and the corresponding tsunami impact has been defined as 'amplified through anthropogenic activity' (light orange colour in Fig. 5). However the pre-existing cleared area did not significantly increase the inundation distance, which remains almost similar for the western part of this zone (in green) as for the eastern part (light orange), and amounts to about 500 m. May the cleared places not have existed before the tsunami, the inundation distance may have been slightly shorter on this specific part of the flooded zone.

Near the longitude 108°52′E, using Quickbird images allows refining the impact estimated from the SPOT5 image (Fig. 6). As previously observed on the SPOT5 image (Fig. 4), the original forest appears as destructed, but several clumps remain standing. The Quickbird image confirms the extent of the inundation, and even defines a larger impact zone characterized by sparse trees, more or less following riverbeds, especially in the western and the eastern parts of this area. Besides, most of the cleared zones on the Nusa Kambangan island seem to correspond to river mouths, as also evidenced further east near longitude 108°56′E where, again, inundation distances amount to 100–200 m, reaching 300 m along riverbeds (Fig. 7).

Without any further information on local elevation values, but assuming average ground slopes similar to Permisan, these first results provide minimum values for the run-up that are actually close to the ones surveyed in the area of the prison. Before synthetizing them in these terms, we first focus on the Permisan area with higher resolution imagery.

2.3 Focus on the impact on the Permisan area

The pre-event SPOT2 image shows that the Permisan prison was surrounded by dense vegetation, with however a possible less thick cover that could correspond to places cleared before the tsunami (Fig. 8), similar to what is also observed elsewhere on the pre-event scene on Fig. 5. For the prison, the SPOT5 image underlines the forest widely cleared after the tsunami, the prison being reached by the tsunami waves, in agreement with field survey observations (Fritz *et al.* 2007). The possibly pre-existing cleared fields are located within the tsunami impact zone, as also evidenced on the Quickbird scene, which allows identifying the field borders. These fields have been defined as amplified through anthropogenic activities, and marked in light orange (Fig. 8, bottom).

The Quickbird image also provides a likely impact in the forest not previously cleared, and which was marked in dark green in

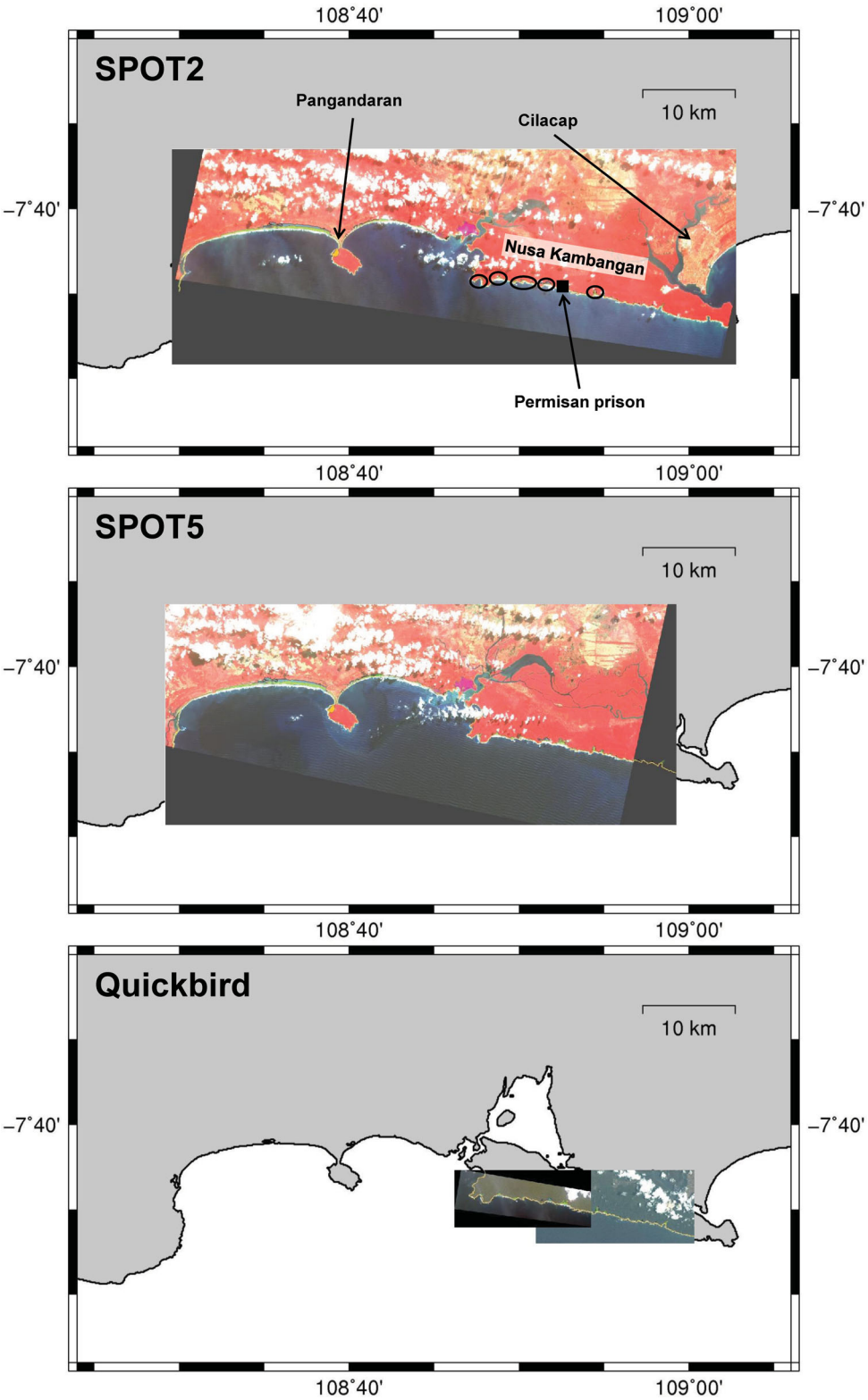

Figure 3. Images used to analyse the coastal impacts, from the pre-event 2006 June 26 SPOT2 scene (top panel) to the post-event 2006 July 22 SPOT5 (centre) and Quickbird scenes (2006 November 27, bottom left, and 2006 November 14, bottom right).

Fig. 8. These places are beyond the assumed pre-existing trimline and may reflect higher altitudes. However their extent even seems to exceed the limit of the extreme measured run-up values (Fritz *et al.* 2007), which correspond very well to the trimline identified on the SPOT5 scene from 2006 July 22 (Fig. 8, top right panel). Since the Quickbird scene dates back from 2006 November, we cannot rule out that 4 months after the event, the debris could have been cleaned and the dead trees cut, so that the zones appearing

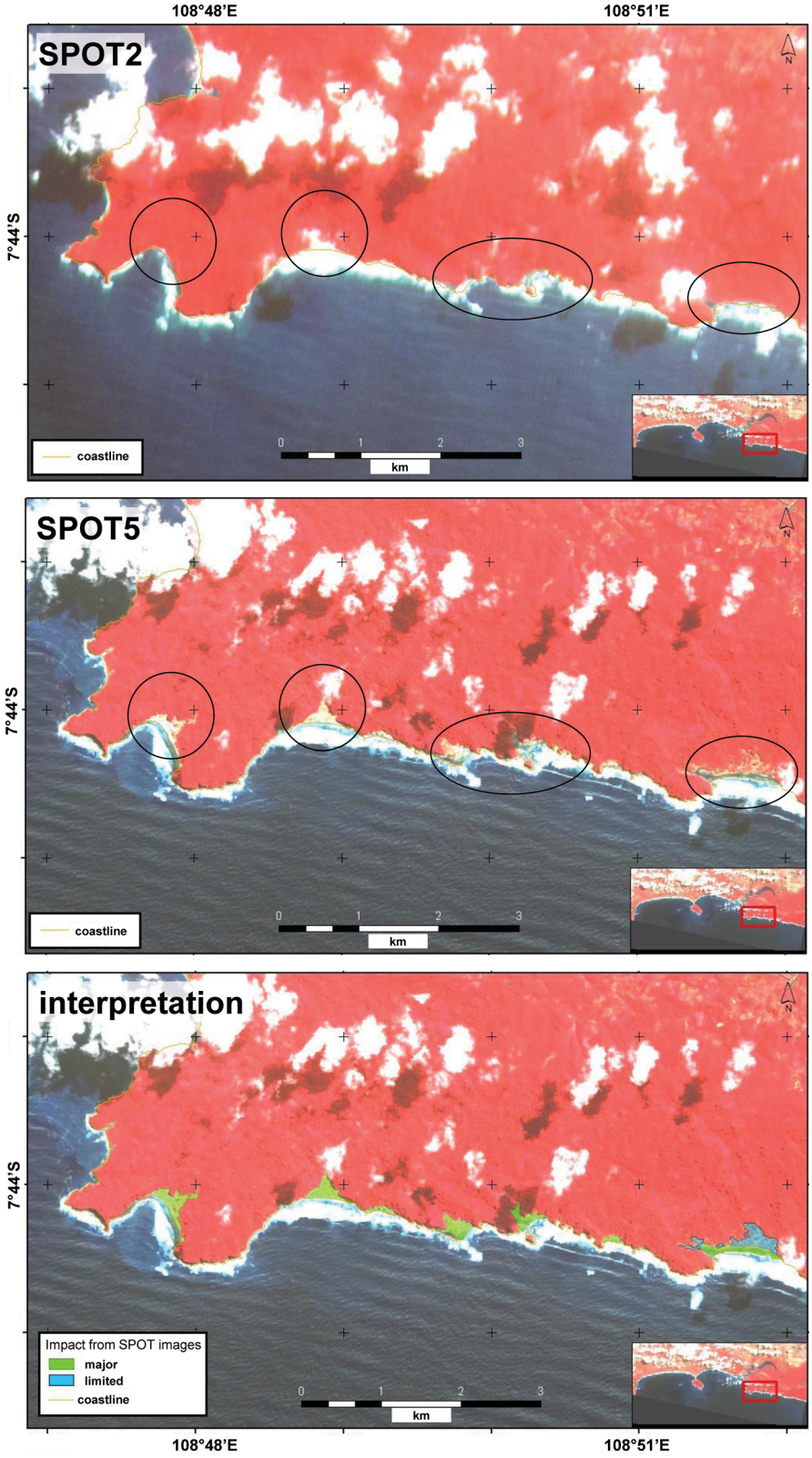

Figure 4. Focus on the western part of the Nusa Kambangan island. Post-event images allow identifying at least four impacted bays with inundation distances from 100 to 300 m. Impact is defined as major (green) or more limited (blue).

as washed by the tsunami may actually correspond to some more recent human activities. Prisoners serving as workers were indeed involved in removing the debris early 2006 August (Fritz, personal communication, 2011).

Similarly to the scene displayed in Fig. 5, we could also propose that the cleared fields before the event (orange colour) helped the tsunami waves to reach the Permisan prison. Nevertheless it is impossible to state that the wild forest provides a natural protection

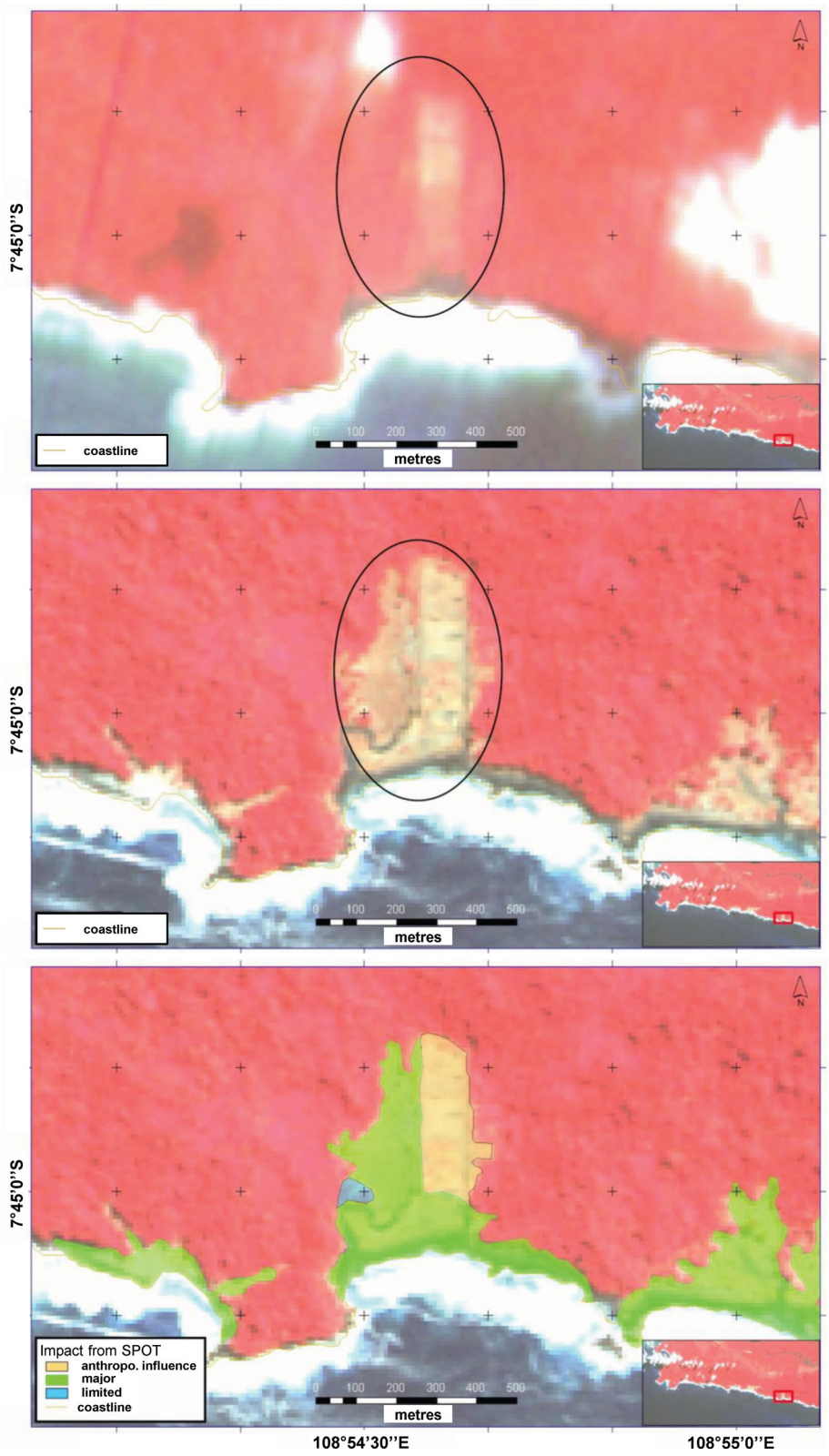

Figure 5. Role of pre-event anthropogenic activities (possibly cultivated fields), identified on SPOT2 (top panel) on the future tsunami impact (SPOT5 image, centre and bottom panels).

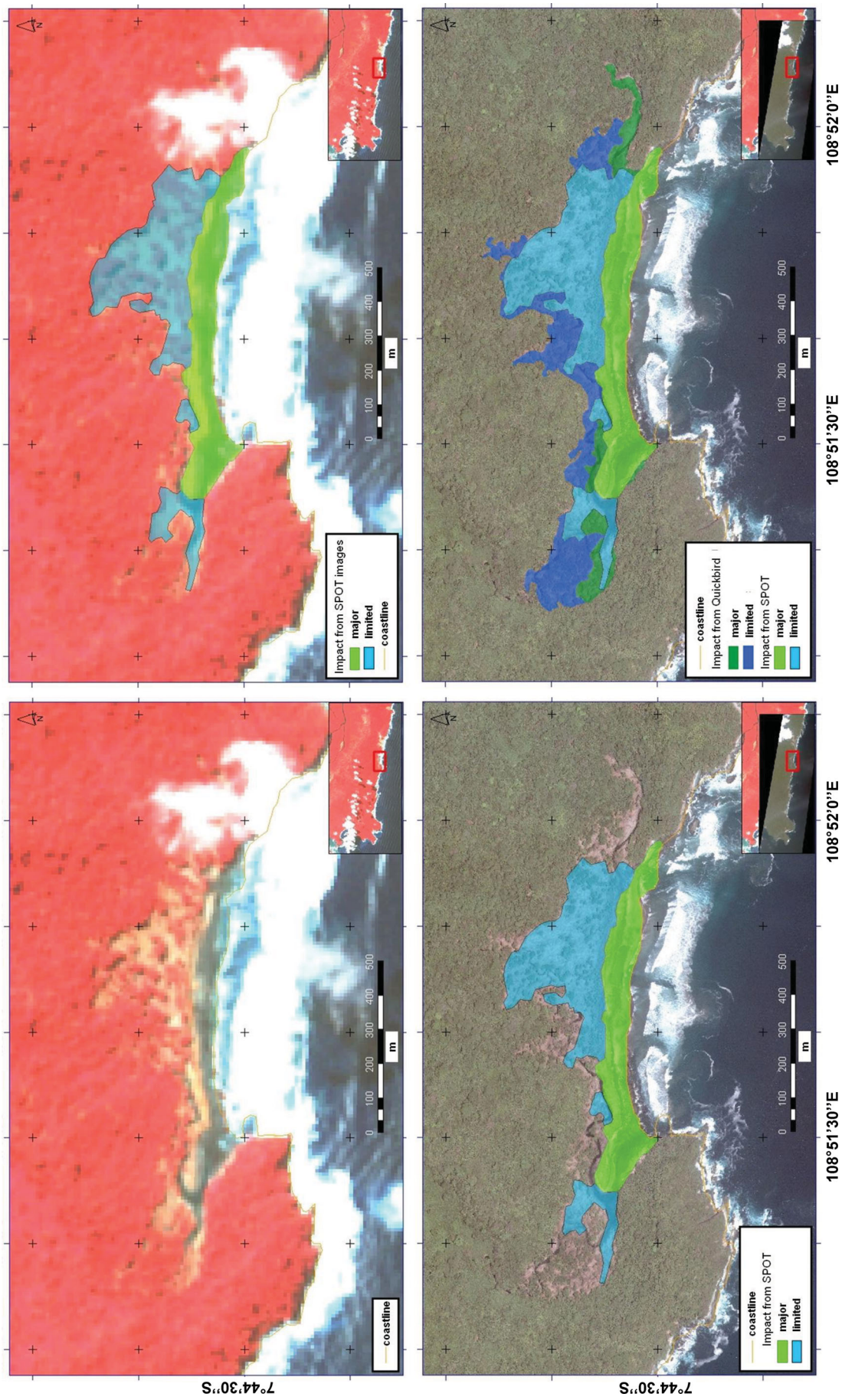

Figure 6. Use of Quickbird images to refine the definition of the impact level near 108° 52′E.

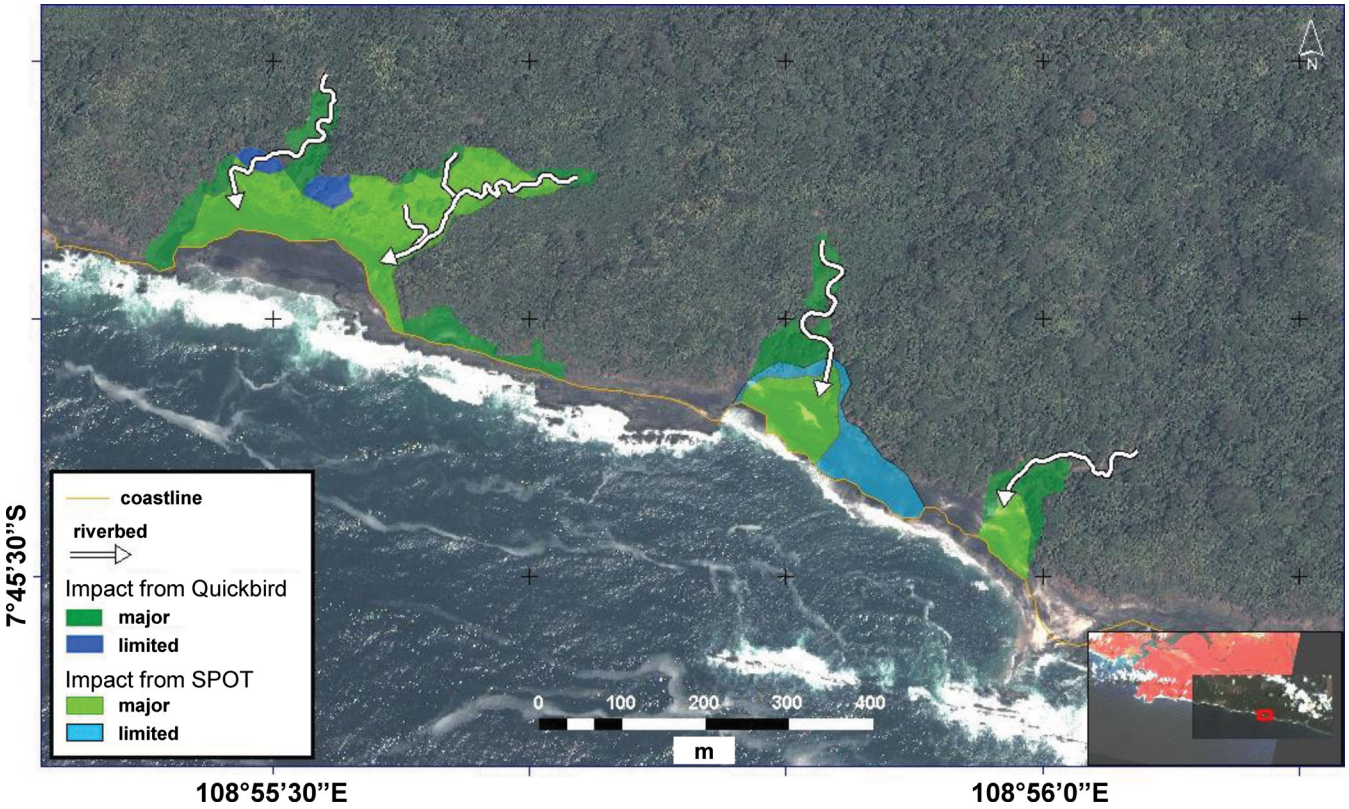

Figure 7. Flooded zones in the vicinity of riverbeds evidenced on the Quickbird and SPOT5 scenes.

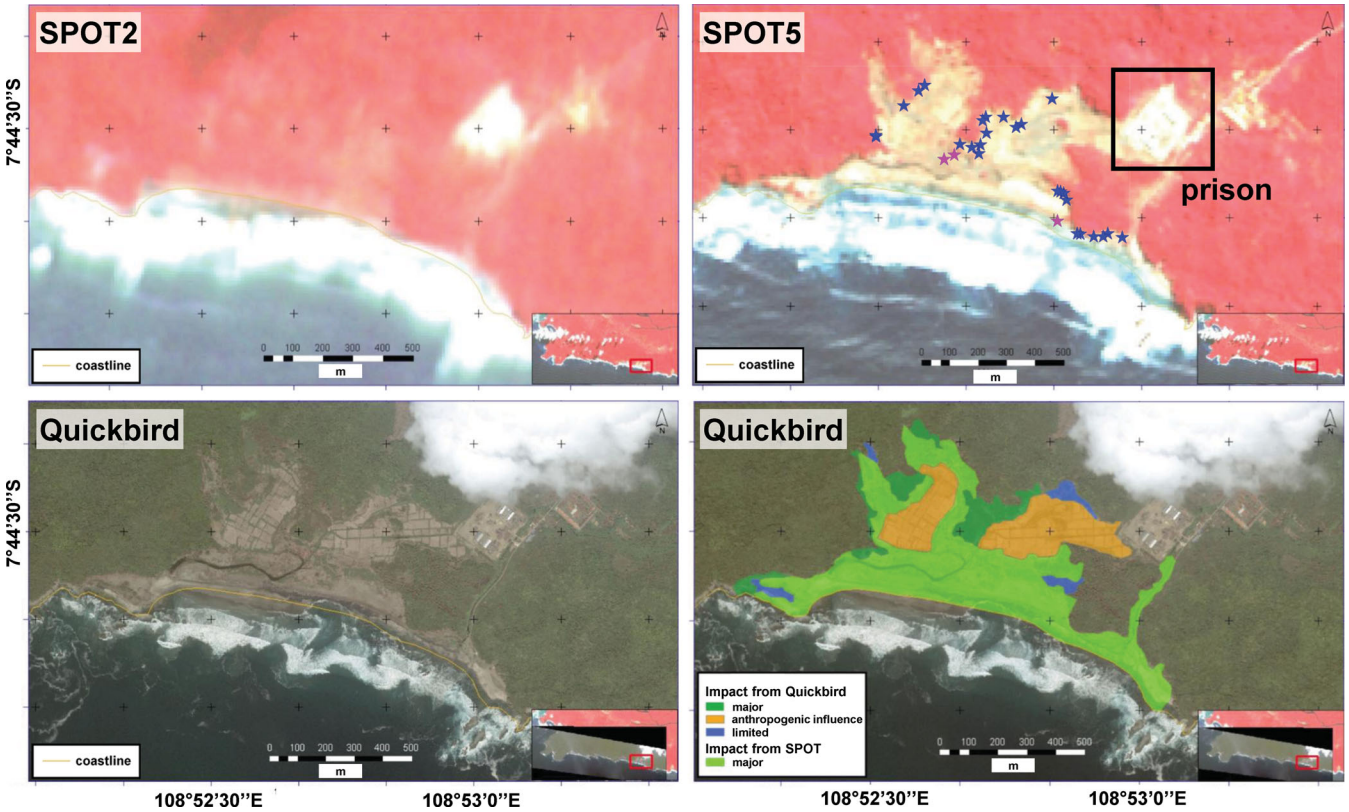

Figure 8. The SPOT2 image reveals possible cleared areas that may have facilitated the flooding, marked in orange in the Quickbird scene. The SPOT5 image confirms how well the run-up (blue stars) and flow depths (pink stars) measured by Fritz *et al.* (2007) fit the trimline.

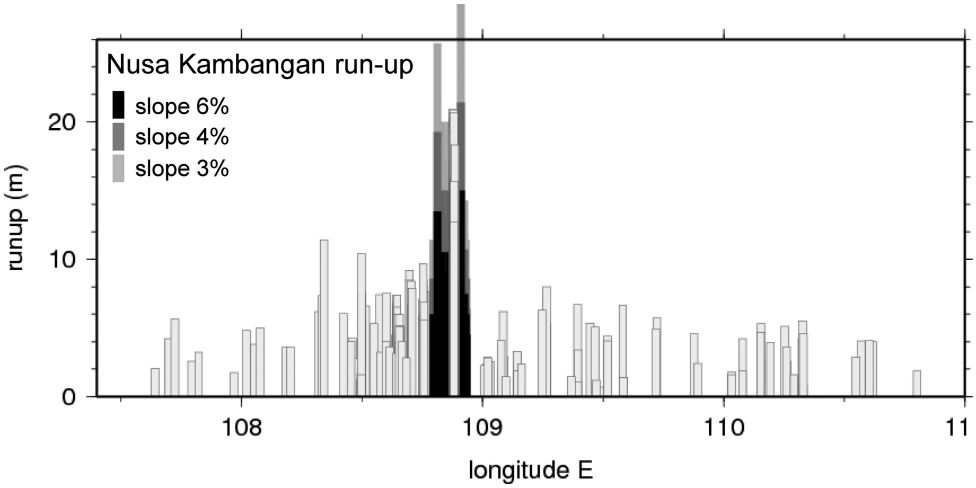

Figure 9. Distribution of the tsunami run-up heights (grey bars) as in Fig. 2, completed by estimates from satellite imagery for the run-up heights near Nusa Kambagan for various average ground slopes.

against tsunami waves, but it could increase the soil roughness and thus contribute to a deceleration of the tsunami flow. Fig. 8 also indicates that the prison may have been reached by tsunami waves through a water canal located to the east, which constitutes a kind of riverbed favouring tsunami penetration, but is also bordered by cleared paths, all these points increasing the tsunami inundation.

All in all, the area near the Permisan prison was heavily struck by tsunami waves, and inundation distances reach about 400 m inland, perpendicular to the shoreline.

2.4 Distribution of tsunami heights

The analysis of satellite imagery reveals long inundation distances all along the Nusa Kambangan shoreline, at several places likely related to the presence of riverbeds. These results confirm the large impact of the tsunami on this island, not only close to the prison, but also at several other places where the inundated area was similar to the one of Permisan. The measured inundation distances range from 100 to 500 m. These results broaden the measures taken on this specific island where access was restricted, and where only one site could be surveyed in the days following the tsunami (Fritz *et al.* 2007).

Retrieving run-up values from these inundation distances implies to know the average ground slopes between the shore and the run-up measurement point. The mean slope in the Permisan area reaches 5–6 per cent, provided the maximum run-up of about 20 m is reached at the measured 350 m distance: this probably yields the maximum possible slope. More reasonably, the slope could range from 3 to 4 per cent. The corresponding run-up heights displayed in Fig. 9 (grey bars) show how the extreme run-up area is extended (about 20 km) within the wider coastal run-up distribution, stressing the particular tsunami impact revealed on the whole Nusa Kambangan island, thus not only on the Permisan prison. Fig. 9 shows that these tsunami heights cannot be compared to the tsunami heights measured elsewhere along this part of Java Island. In the following we are discussing this distribution with the help of tsunami modelling.

3 METHOD AND DATA USED FOR TSUNAMI MODELLING

We use numerical modelling to compute tsunami initiation, propagation and run-up on different coastal places. Different seismological sources are tested to model the sea bottom coseismic deformation triggering the tsunami. We compare our modellings with the outstanding video recording of the wave arrival in the PLTU Power Plant east of Cilacap that was converted into a tide gauge record (Lavigne *et al.* 2007). Run-up computations are then focused on the Permisan area where a refined DEM has been established thanks to satellite imagery.

3.1 Method

The method used to model tsunami waves follows the approach solving the hydrodynamic equations under the non-linear shallow water (NLSW) assumption (Heinrich *et al.* 1998; Hébert *et al.* 2001, 2007). The method solves the depth-averaged NLSW hydrodynamic equations with a finite difference scheme working on staggered grids that describe for each gridpoint the propagation velocity $c = \sqrt{gh}$, where g is the gravity acceleration and h the water depth. The tsunami initiation comes from the perturbation of the sea bottom in response to the displacement due to the earthquake. This initial deformation is computed through a model of elastic dislocation (Okada 1985) constrained with seismological parameters of the rupture that verify the expression of moment magnitude $M_0 = \mu ULW$, where μ is the rigidity, U the average slip amount, L the length and W the width of the fault plane (e.g. Kanamori & Anderson 1975). When taking into account a finite rupture propagation, which is worth being tested for slow tsunami earthquakes, the contribution of each subfault is computed at the corresponding rise time, and added to the ongoing wavefield.

The hydrodynamical equations are:

$$\frac{\partial (\eta + h)}{\partial t} + \nabla \,.\, [\mathbf{v}\,(\eta + h)] = 0, \tag{1}$$

$$\frac{\partial (\mathbf{v})}{\partial t} + (\mathbf{v} \,.\, \nabla)\,\mathbf{v} = -\mathbf{g}\nabla\eta, \tag{2}$$

where h is the sea depth and η the water elevation above mean sea level, $\mathbf{v}$ the depth-averaged horizontal velocity vector, $\mathbf{g}$ the gravity acceleration. Equations of continuity (1) and motion (2) are solved in spherical coordinates by means of a finite-difference method, centred in time and using an upwind scheme in space. Under the shallow water theory dispersive effects are neglected. Close to the

coasts the phase velocity $c = (gh)1/2$ drastically decreases, leading to the tsunami wave amplification.

The decreasing of tsunami wavelengths implies the need for finer bathymetric grids when the tsunami approaches the coasts. To properly model the tsunami arrival at the local scale we usually consider a series of five levels of nested bathymetric grids characterized by an increasing resolution, from a few kilometres in deep ocean (encompassing the source area) down to 5–15 m in bays and harbours. Open free boundary conditions are ascribed to the boundaries of the larger grid, and wave heights and velocities along the boundaries of a fine grid are spatially interpolated at each time step from the values computed in the coarse grid containing the fine grid.

3.2 Building a DEM

To compare tsunami observations with modelling, we took the opportunity to have high-resolution images in the area of the prison to build a detailed DEM essential for refined tsunami modelling. To this aim we needed a couple of high-resolution images taken after the tsunami, to map the area on both scenes, and without vegetation. We added a Quickbird image from 2006 December 7 to the previous image from 2006 November 27 to build a stereoscopic pair taken at different incidences. The first image (November 27) was taken with a 106° azimuth and a 69.9° incidence, while the second image (December 7) had a 275° azimuth and a 72.1° incidence, thus this couple offers an optimal stereoscopic view, with a base to height ratio of $B_h = 0.7$.

About 450 tie points have been manually identified on both images (Fig. 10), first close to the shore where the ground without vegetation was available, then on most of the cleared places. Then the relative altitudes were computed through the parallax estimation between both scenes. Since QuickBird images are orthorectified with a constant mean height DEM (ortho-ready products), the parallax Δp along the epipolar direction between the images is related to the relative altitude to the orthorectification mean height Δh by:

$$\Delta p = \Delta h * B_h + K, \tag{3}$$

K being an unknown bias related to the global misregistration of the images. The few relative heights obtained within the forest have been corrected from a standard palm tree height taken to 13 m. The obtained values have also been cautiously adjusted to the available run-up values obtained in the area (Fritz *et al.* 2007), which also provide altitudes at the surveyed places. The final interpolation was carried out with additional data taken from SRTM values above the 20 m altitude.

Concerning bathymetric data, no detailed nautical chart was available. We chose the trend from the GEBCO 30″ data (IOC, IHO & BODC 2003) that were progressively re-interpolated close to the studied site, to produce a complete computational grid imbricated to a series of five regular grids, from a 1′ (about 1800 m) grid encompassing the earthquake source, down to the final 15 m grid focusing on the Permisan area. In the following we show the results of tsunami modelling towards this place, as well as towards the area of PLTU Power Plant east to Cilacap.

3.3 Bathymetric grids for this study

We based our bathymetric grids on the global bathymetry now made available at a 30″ cell size (GEBCO data, IOC, IHO & BODC 2003). The first grid level (extent of Fig. 1) was built from a 1′ sampling of these data, enough to discretize the source rupture area and to enable rapid computations. Then subsequent grid levels have been synthetized using interpolations of containing values and more refined data sets. The grids 2 (extent displayed in Fig. 2), 3 and 4 focus on the Permisan area down to a 15 m grid cell corresponding to DEM data constructed from stereoscopic imagery (Fig. 10). While these topographic data are here well detailed, no refined bathymetric data were available off the Permisan area. We added bathymetric contours from the GEBCO 30″ data to ensure a proper focusing and imbrication of the bathymetric grids. However it has to be noted that, while the average slope offshore is probably well modelled this way, the detailed local coastal features are not taken into account in this grid.

Concerning the PLTU area, a 45 m grid was built based on additional data for the Cilacap harbour, provided by local authorities. At the PLTU site, available pictures of the water supply channel and observations reported by field surveys (Lavigne *et al.* 2007) allowed digitizing a bathymetric data set that was interpolated into a 15 m grid to model the channel. Although this is a rather coarse approach, and topographic data were not considered here (their trend was taken

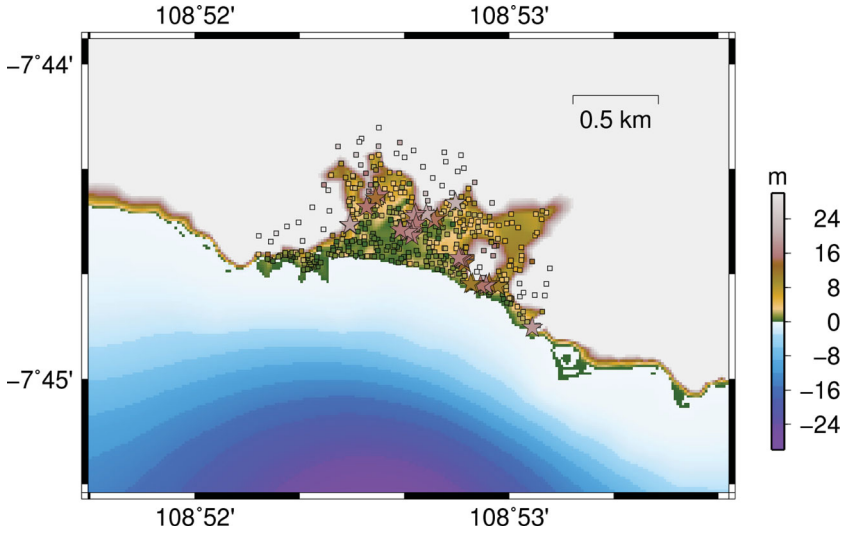

Figure 10. Topographic model of the Permisan area, completed with bathymetry derived from GEBCO data. Coloured squares show the points extracted from stereographic analysis of the couple of Quickbird images.

from SRTM data), the overall dimensions and depth of this basin appearing in the video recording are well reproduced using direct witnesses reports (Lavigne, personal communication, 2006).

3.4 Earthquake sources

We chose to test available seismological sources for the 2006 earthquake, first a source computed through an inversion of Rayleigh waves confirming the slow rupture and the directivity towards an azimuth of 109°E (Ammon *et al.* 2006), and second, a source based on the inversion of tsunami waveforms recorded at several places in the Indian Ocean (Fujii & Satake 2006). This kind of tsunami data inversion has proved to be consistent with seismological models retrieved from inversions of seismic data, and are able to produce similar patterns of coseismic slip heteorogeneities for large earthquakes (Sladen & Hébert 2008); besides joint inversions using both tsunami and seismic data sets are nowadays frequently carried out to produce consistent coseismic models, as for the 2011 Tohoku earthquake (e.g. Yokota *et al.* 2011).

The first model used here (Ammon *et al.* 2006) involves a very low rigidity of 10 GPa consistent with a rupture within the sedimentary accretionary wedge, a common characteristic inferred for tsunami earthquakes (Polet & Kanamori 2000), and the rupture velocity is retrieved to 1.25 km s^{-1}. Distributed over 975 subfaults with an average slip of 8–15 m, this model yields a seismic moment of 7.0 10^{20} Nm.

The tsunami waveform inversion (Fujii & Satake 2006) yields, first, the area of the source rupture, and, second, a slip distribution over 10 subfaults. By letting both the rupture velocity and the slip distribution vary, the resulting source model consists of average slips from 0.5 to 2.5 m, assuming a rigidity of 30 GPa.

In the following we test both source ruptures using infinite rupture velocities (static model), and then finite ruptures. Initial seafloor deformations taken at 0 s (infinite rupture) or after 400 s (finite rupture) reveal that the Ammon source (Fig. 11, top) produces higher wave amplitudes than the Fujii source (Fig. 11, bottom).

4 RESULTS FROM TSUNAMI MODELLING

4.1 On the regional scale

Modelling results at the regional scale (Fig. 12) confirm the great values of tsunami heights obtained using the Ammon model. For this source indeed, maximum tsunami heights computed offshore reach 2 m and more for three distinct areas: the whole margin off Pangandaran, the island of Nusa Kambangan and the bay of Cilacap. Actually two of these maximum lobes already originate farther offshore, from the source, beyond the main margin slope, and they are eastwards shifted when a finite rupture velocity is considered (model B). As expected, using a rupture velocity can change the tsunami pattern offshore, as already shown for example for the 2004 tsunami (Geist *et al.* 2007), and this can change the definition of areas at risk. However, for the 2006 tsunami, as the studied area is in the near field, the impact seems to be only marginally shifted from a few kilometres. The three maximum lobes evidenced here are also correlated with three shallower parts of the breaking slope, hence low-velocity zones acting as focusing lenses, where tsunami heights are more amplified.

A similar tsunami pattern is obtained for the Fujii source (models C and D), even though with smaller amplitudes. In the latter case however, the finite rupture even yields larger amplitudes off PLTU than off the prison, for an unclear reason. Except for this area, the amplitudes computed offshore do not exceed 1 m.

All conducted models allow defining the area from Pangandaran to east Cilacap as the most impacted area. This portion of the coastline also seems to correspond to a wider margin shelf (between 108.5°E and 109.5°E), seemingly less steep than the other coastal shelves farther westwards and eastwards. This pattern may be able

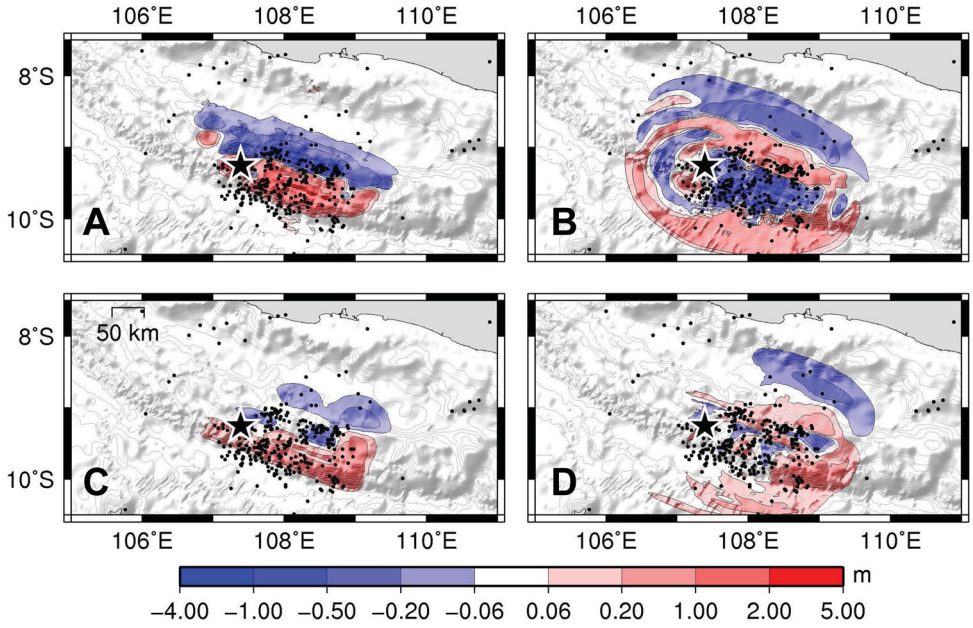

Figure 11. Earthquake sources used: (A) the rupture model obtained from the seismological inversion carried out by Ammon *et al.* (2006), using an infinite rupture; (B) the same with a 1.25 km s^{-1} rupture velocity, after 400 s of eastward rupture; (C) the model from the tsunami inversion done by Fujii & Satake (2006) with an infinite rupture velocity and (D) the same with a rupture velocity of 1 km s^{-1}, after 400 s of eastward rupture. Black dots show aftershocks from USGS during 1 yr after the main shock (plotted as a black star).

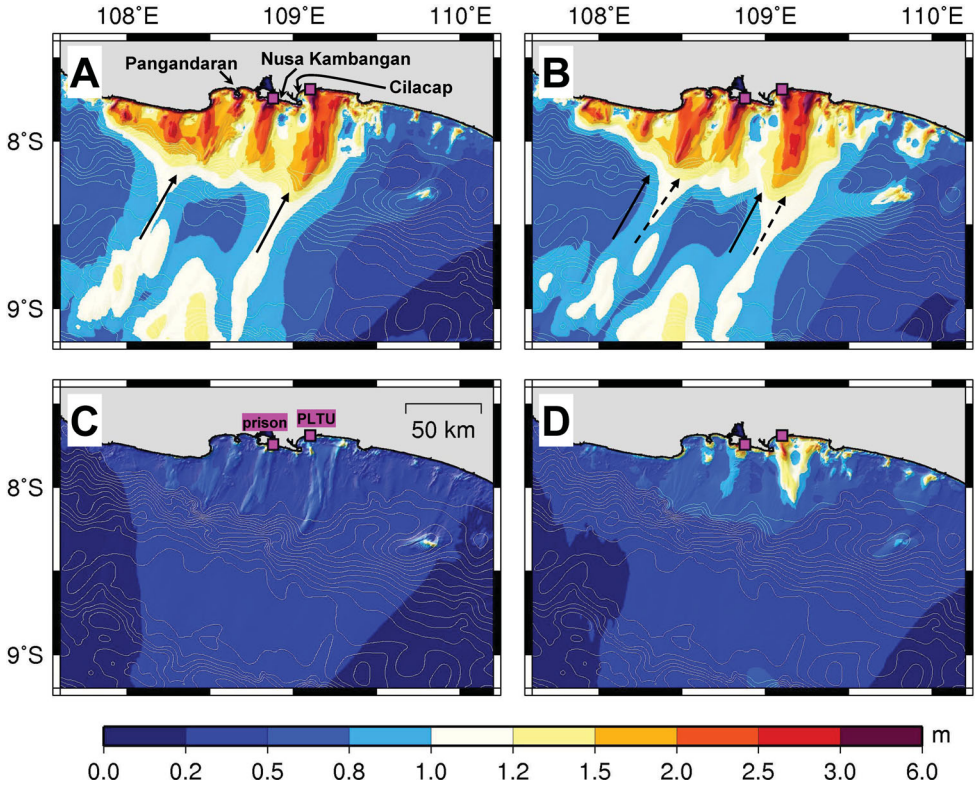

Figure 12. Maximum tsunami heights computed offshore for the four earthquake sources, after 2 hr of propagation. White dashed lines are bathymetric contours plotted every 250 m. Pink squares display the locations of the Permisan prison (west) and the PLTU power plant (east). Kinematic source models (B and D) shift the maximum tsunami amplitudes eastwards from a few kilometres. Arrows denote these maximum values computed offshore for the static model A (solid arrow) and the kinematic model B (dashed arrow).

to keep the tsunami energy and even to efficiently amplify it before reaching the coast for the whole impacted area.

4.2 Comparison with observations in PLTU

The video recording in the PLTU basin was converted in a sea level temporal variation (Lavigne *et al.* 2007) and can be compared with modelling results. All the source models yield a very satisfying waveform for the gauge located where the sea level was observed on the record.

Using static source models (Fig. 13, bottom) yields first arrival times slightly in advance with respect to the observation, with a shift from 5 min (Fujii source) to 4 min (Ammon source). The modelled amplitudes are larger than the observed one for the Ammon source (5 m compared to about 3 m), while the Fujii source is too small with a factor of about 2. However, the waveform is satisfactorily close to the one recorded, and the models predict a second wave arriving about 12 min after the first one. This wave was indeed reported by several witnesses in the area of Cilacap.

Using a finite rupture increases the modelled amplitudes with the Fujii model, as for the model in the Permisan area, while the Ammon source similarly exceeds the observation (Fig. 13, top). The arrival times are also closer to the observed ones, especially for the Ammon model: as expected from the source directivity, the kinematic models increase the arrival times of about 2–3 min. For all models the computed duration of the first arrival is about 8 min, to be compared to the observed 10 min duration. Subsequent waves were not reported from the video recording, while the models indicate further arrivals of smaller amplitude about 12 min after. It is also worth stressing that the very abrupt inception of the wave is well modelled and similar to the observed one.

These results illustrate the efficiency of the Ammon source, and to a lesser extent of the Fujii source, to match the tide gauge observations. Even though the used DEM is approximate, the basin geometry has been cautiously designed to be consistent with the actual one, allowing to properly model tsunami amplitudes. However since the approach of the basin may be more inaccurate, this could account for the time shift observed between the synthetic and actual signal. Such shifts are not unusual in detailed tsunami modellings and synthetics are often earlier than observations since the velocity model does not account accurately for the shoaling effect in the last metres, where this is the most influent.

4.3 Detailed study in the Permisan area

The computation was also refined in the vicinity of the Permisan prison, using the 15 m DEM built from satellite imagery. All of the tested source models yield a substantial flooding of the whole area close to the prison, but amplitudes significantly vary depending on the source (Fig. 14). As already indicated by the results offshore (Fig. 12), the Fujii static model (C) produces too low amplitudes, yielding run-up heights not exceeding 2–3 m, while the Ammon static model (A) produces a satisfying inundation pattern, yet with computed amplitudes lower than the observed ones. More in detail, the computing maximum tsunami heights using this latter model only reach 10 m at most. The map view indicates that the observed run-up points are reached by the water, reflecting how the DEM may be characterized by such high slopes close to the measured

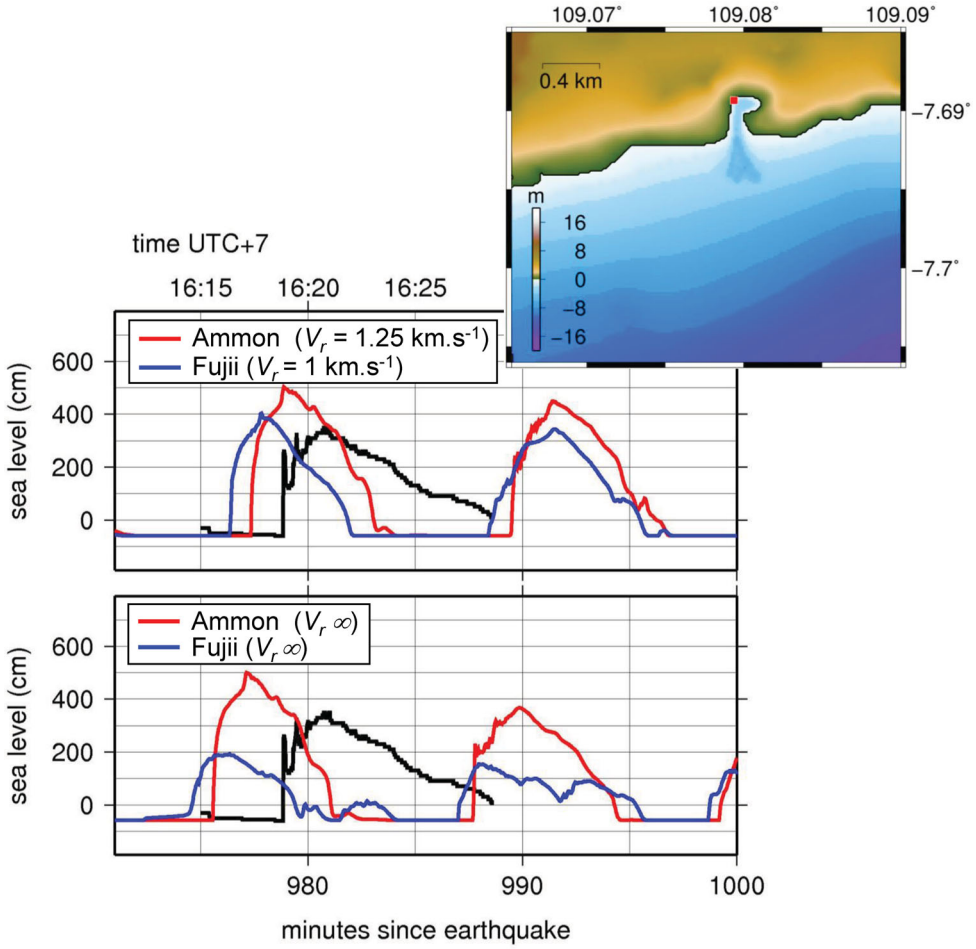

Figure 13. Modelling results for the PLTU basin, which coastal bathymetry is shown up right. The sea level variations observed from the video recording are plotted in black. The synthetic signals computed at the gauge displayed with a red square (see insert) are plotted for the different earthquake sources, using finite (top) and infinite (bottom) source rupture velocities.

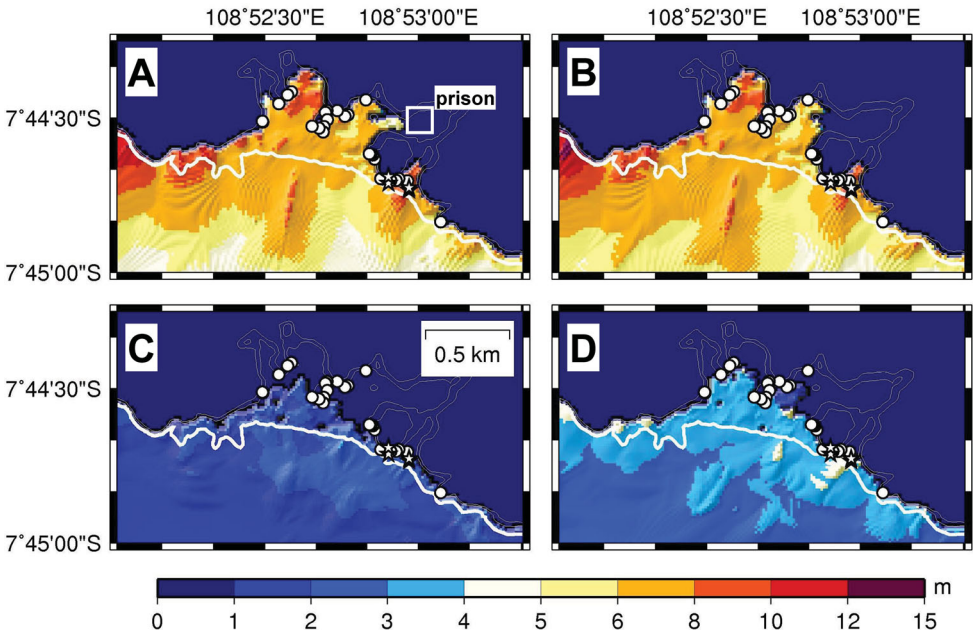

Figure 14. Maximum tsunami heights computed in the Permisan area, for the four earthquake sources, after 2 hr of propagation. The shoreline at rest is displayed with the thick white line. White dots show the tsunami run-up data gathered by Fritz *et al.* (2007), and white stars are tsunami data collected by Lavigne *et al.* (2007).

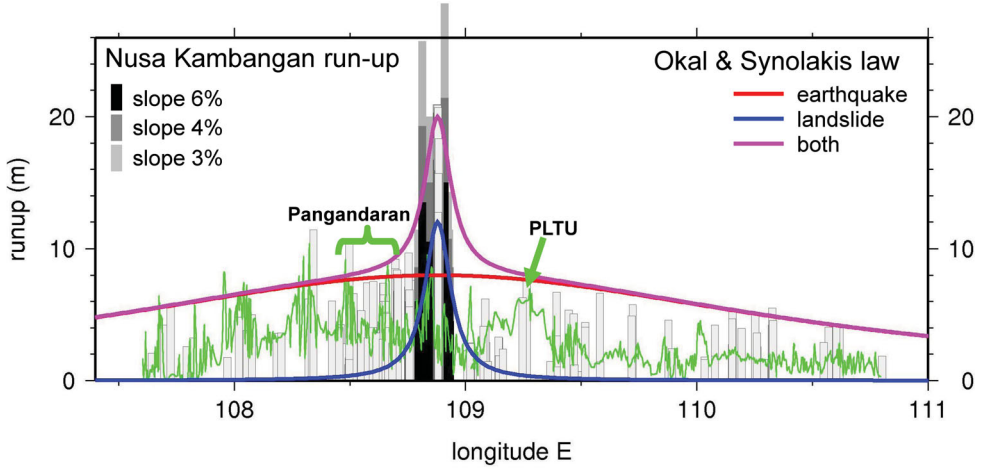

Figure 15. The exceeding tsunami heights in the area can be explained through an additional tsunamigenic source as modelled using the Okal & Synolakis (2004) law. The green line is the result from tsunami modelling, using the Ammon *et al.* (2006) static source, taken along the 5 m bathymetric contour.

run-up that they are actually not reached in altitude by the computed inundation (flow depths reach 5 m and more for the Ammon model).

Using a kinematic model does not change the flooding pattern that significantly, except for the Fujii source. The Ammon source (B) is very similar to the static source (A), apparently more restricted close to the prison. Using the Fujii source (D) increases the flooded area obtained with the static source, reaching the run-up measurement points, but the overall amplitudes are still low, and the flow depths do not exceed 1–2 m.

We conclude that the tested earthquake source able to fit the inundated area is the Ammon source, whatever the rupture velocity, since both kinematic and static models yield the same inundation pattern. The Fujii model seems to produce models about half the results obtained with the Ammon model, as was also observed in PLTU. In the latter case however, using a finite rupture (Fig. 13, top), the Fujii model was closer to the Ammon model. This may be owed to a greater tsunami energy originating from the eastern part of the fault in the Fujii source, as already observed in the offshore results (Fig. 12, model D).

However, in any case, none of these earthquake source models is able to produce tsunami heights comparable with the ones available from field surveys (Fritz *et al.* 2007) that reached about 10 m of flow depth over the inundated area of Permisan. This underlines a need for a secondary source able to fill this gap for this portion of the coastline.

4.4 Modelling the tsunami heights distribution

The distribution of tsunami run-up data along the coastline shown in Fig. 9 can also provide indications on the tsunami source process, especially as it concerns the ratio between the maximum amplitudes and the lateral extent of the distribution along the shore (Okal & Synolakis 2004). This ratio is indeed greatly increased from 10^{-5}–10^{-4} for most of the earthquake sources to 10^{-3} at least for assumed landslide sources (for instance 1946, Aleutian; 1998, Papua New Guinea, both events characterized by an earthquake followed by a large submarine landslide). Following the quantitative description of this behaviour proposed by Okal & Synolakis (2004), we attempted here to model the 2006 distribution using their dimensionless parameters, namely a (lateral extent of sustained run-up along the coast), b (maximum run-up height), defining $I_2 = \frac{b}{a}$ as the aspect ratio of the distribution, and,

(1) for an earthquake, $I_1 = \frac{b}{\Delta u}$ where Δu is the fault slip,
(2) for a landslide, $I_3 = \frac{-b}{\eta_-}$, where η_- is the initial depression of the sea surface.

For the 2006 data, the overall distribution is well modelled using $a = 200$ km, $b = 8$ m and $\Delta u \sim 6$ m. This yields $\log(I_1) = 0.1$ and $\log(I_2) = -4.4$, thus in the upper category of the series of modelling results displayed in Okal & Synolakis (2004) study, consistent with tsunami earthquakes such as in 1994 (Java) or 1992 (Nicaragua). The corresponding red line displayed in Fig. 15 obviously cannot explain the peak amplitudes of the Nusa Kambangan island. An additional source described by $a = 8$ km, $b = 12$ m and $\eta_- = 9$ m, corresponds to $\log(I_2) = -2.8$ and $\log(I_3) = 0.1$, and again belongs to an extremity of the modelling results of the referred study. The corresponding blue line in Fig. 15 allows to propose a very narrow run-up distribution which, added to the previous one, is able to properly explain the overall distribution reaching about 20 m in its centre (pink line in Fig. 15). This is consistent with the additional source already proposed (Fritz *et al.* 2007), that we finally also proposed from the modelling results presented in the previous sections.

5 DISCUSSION AND CONCLUSIONS

5.1 Discussion on the uncertainties

While satellite imagery provided a clear horizontal mapping of the flooded areas, we saw that the uncertainties on the average ground slope are not large enough to discard a striking anomaly in the run-up distribution along the coast. Tsunami modelling can also be associated with uncertainties, especially concerning the source model used and the flooding parameters. However tsunami studies relying on modelling are generally efficient to discuss the characteristics of an event based on run-up data, or tide gauge data when available. For instance, tsunami modelling can efficiently explain observed sea level anomalies in the far distances, provided accurate bathymetry is available in the harbour, and all the more as an accurate model of the slip heterogeneities is used (examples in La Réunion, Hébert *et al.* 2007, or in French Polynesia, Hébert *et al.* 2009). A single source model is however rarely relevant (see for instance Poisson *et al.* 2011), and the definition of the source parameters also depends on the propagation model used: source components of shorter wavelength may require a model taking into

account frequency dispersion. In our study, close to the source, such dispersion cannot be significant, and the source wavelengths are long enough to avoid a dispersive model.

Nevertheless, high-resolution bathymetric data are necessary to improve models near Permisan. In this study, in designing an elevation model from satellite imagery, we achieved to produce tsunami models using realistic earthquake sources. These input parameters remain at the origin of the first-order uncertainties in the results, as shown using either the Ammon or the Fujii source. Even with a more realistic source accounting for the 2006 low seismic rupture, such results in the near field are not significantly changed. Such an effect is expected to be more influencing in the far field, when maximum tsunami energy can be significantly shifted in the direction of the seismic rupture (Geist *et al.* 2007; Poisson *et al.* 2011).

The modelling of flooding is very sensitive to various parameters of the models. However, generally, models tend to overestimate the flooding because they lack physical dissipation due to the ground friction. In our case, this is unlikely to occur, because the extent of the flooding is not questionable, and by the way is rather well modelled. Instead these are the overall modelled flow depths that remain too low by a factor 2 at least, with respect to observations, thus again stressing the need for a more complex source.

5.2 A possible secondary source

Our refined modelling provided a good inundation pattern on the Permisan area (Fig. 14), with flow depths from 2 to 5 m, however the computed run-up heights do not exceed 10 m. Thus these values remain smaller than the observed flow depths (about 10 m) and the run-up heights (about 20 m) for this Permisan location. By contrast, using the same earthquake and tsunami modelling for the PLTU site provides water heights more consistent with the observations (Fig. 13).

Coarse modelling results obtained using the earthquake source from Ammon *et al.* (2006) are also displayed in Fig. 15 (green line). They are taken along the 5 m bathymetric contour, and exhibit amplitudes from 2 to 6 m, in line with the overall data distribution. These figures are consistent with coastal amplitudes reaching finally 10 m and even more, once the shoaling effect is taken into account. However the peaks obtained in this coarse modelling do not indicate a specific relative amplification towards Nusa Kambangan, but rather towards Pangandaran and PLTU sites, which were indeed heavily impacted (Lavigne *et al.* 2007).

Whenever an additional tsunami source has to be invoked, as already suggested in previous studies (Fritz *et al.* 2007; Lavigne *et al.* 2007), our study confirms that it should have occurred directly off Nusa Kambangan, where it may have doubled the final tsunami amplitudes along a portion of the coastline not exceeding 20–30 km in length. Following the analysis presented, a tsunamigenic landslide with an initial depression η_- close to 10 m could have been triggered there. This scenario is significantly smaller than a similar sequence (earthquake followed by a submarine landslide) in 1998 in Papua New Guinea (Heinrich *et al.* 2001) that produced extreme run-up values along about 20 km of the shoreline, while tsunami heights barely reached 1–2 m, 20 km away from this extreme height. To a less extent, the tsunami triggered in 1979 by a submarine failure off the Nice airport (French Riviera) produced extreme tsunami heights (at least 5 m) at the airport, while it was unnoted on a tide gauge located 15 km away in Mandelieu (Labbé *et al.* 2012). On the contrary in 2006, the earthquake source alone still contributes to high tsunami waves more than 50 km from the maximum amplitude point.

Such a secondary source off Nusa Kambangan could therefore have contributed to increase run-up on the Nusa Kambangan island only, while other places would have been impacted by the tsunami essentially due to the earthquake, which, as a tsunami earthquake, produced large water heights for this level of magnitude. Also, in the case of this 2006 tsunami earthquake, which is supposed to have radiated low-frequency seismic waves, with a soft ground shaking, the triggering of a landslide should have occurred in submarine slopes either very steep and/or very unstable. One could also remark that in 2006 May a strong earthquake shook central Java with magnitude M_w 6.2, less than 200 km away from the 2006 July earthquake. Submarine sedimentary layers on steep slopes could have increased their instability at the occasion.

The recent synthesis of bathymetric data in Indonesia (Brune *et al.* 2010) reveals important submarine landslides, one of them offshore Java, with an assumed 3 km^3 volume, but far eastwards of Pangandaran near 110°30′, thus not realistically related to the 2006 July tsunami. According to Brune *et al.* (2010), submarine landslidings are frequent off Indonesia, and the important sedimentary deposition may even be oversteepened by tectonic processes due to subduction, especially off Java.

In any case, only a detailed *in situ* investigation off Pangandaran and Nusa Kambangan (high-resolution bathymetry and subbottom profiler) could complete the surveys presented in this synthesis of landslides identified off Java (Brune *et al.* 2010), and confirm whether such an event may have occurred in 2006. This would also be fruitful to better characterize the submarine slopes off Nusa Kambangan, and the capacity of the submarine relief to focus or defocus tsunami energy. The available bathymetric data from global data sets do not reveal any tsunami-focusing feature, such as a localized submarine ridge. The impact of this kind of structure is however important for high water depths (a few hundreds of metres), where more important relative velocity contrasts are more efficient in focusing and defocusing the tsunami energy. The continuous improvement of the global bathymetry data sets makes rather unlikely that such a structure could be nowadays discovered.

5.3 Concluding remarks

In this study we have been able, thanks to satellite imagery, to image the horizontal extent of the 2006 tsunami on the Nusa Kambangan island, the area where the impact was the highest. Given average ground slopes, these extents confirm extreme run-up values from 15 to 20 m for the whole Nusa Kambangan island, thus not only on the Permisan prison. These satellite data are extremely important to be gathered in the first days after the event, not only to guide rescuing operations, but also to assess damage and to propose DEMs, provided a recent pre-event image is available.

Tsunami modelling carried out for two detailed areas, in the Permisan prison and the PLTU Power Plant, provides contrasted results with respect to available observations, rather underestimated in the highly impacted Permisan site, while rather in good agreement in the PLTU location. Using two published seismological sources, accounting for finite or infinite seismic rupture, these differences cannot be simply explained by modelling uncertainties. However, they confirm that the tsunami was high on all the impacted area, for the magnitude level of the vent, as is expected for a tsunami earthquake. Besides although the dissemination and communication systems have been improved in Indonesia, as well as the automatic estimation of the magnitude in the first minutes after the main shock (Hanka *et al.* 2010), this 2006 event stresses the difficulty

of handling slow earthquakes in the near field in Warning Systems, which must be able to detect the slow seismic rupture involved in such earthquakes, using seismic wave analyses at longer period (Kanamori & Kikuchi 1993).

Following a previous study (Fritz *et al.* 2007), and together with the overall analysis of the tsunami observations along the coastline, our results finally supports that an additional source, possibly due to a submarine landslide, may have increased the tsunami impact off Nusa Kambangan. Only a detailed offshore mapping of the submarine slopes off this region of Java could help confirming such a landlslide source, and would provide essential parameters to compare future landslide modellings with available data.

ACKNOWLEDGMENTS

This work has been supported by the French Agence Nationale de la Recherche, under the contract Cattell TSUMOD ANR-05-CATT-016-01, and then under the contract RiskNat MAREMOTI ANR-08-RiskNat-05. It also initially benefited from the support of the Délégation Interministérielle chargée de l'aide Post-Tsunami (DIPT) set up by the French Ministry of Foreign Affairs after the catastrophic 2004 Indian Ocean tsunami. We thank Hermann Fritz and an anonymous reviewer for their constructive remarks, and the Editor Saskia Goes for her in-depth analysis to improve the clarity of the paper.

REFERENCES

Abercrombie, R.E., Antolik, M., Felzer, K. & Ekström, G., 2001. The 1994 Java tsunami earthquake: slip over a subducting seamount, *J. geophys. Res.,* **106,** 6595–6608.

Ammon, C.J., Kanamori, H., Lay, T. & Velasco, A.A., 2006. The 17 July 2006 Java tsunami earthquake, *Geophys. Res. Lett.,* **33,** L24308, doi:10.1029/2006GL028005.

Bird, P., 2003. An updated digital model of plate boundaries, *Geochem. Geophys. Geosyst.,* **4,** 1027, doi:10.1029/2001GC000252.

Borrero, J., 2005. Field data and satellite imagery of tsunami effects in Banda Aceh, *Science,* **308**(5728), 1596, doi:10.1126/science.1110957.

Brune, S., Babeyko, A.Y., Ladage, S. & Sobolev, S.V., 2010. Landslide tsunami hazard in the Indonesian Sunda Arc, *Nat. Hazards Earth Syst. Sci.,* **10,** 589–604.

Chen, P., Liew, S.C. & Kwoh, L.K., 2006. Tsunami damage mapping and assessment in Sumatra using remote sensing and GIS techniques, in *Proceedings of IEEE International Conference on Geoscience and Remote Sensing Symposium,* 2006 July 31–August 4, Denver, CO, pp. 297–300, doi:10.1109/IGARSS.2006.81.

Fritz, H.M. *et al*., 2007. Extreme runup from the 17 July 2006 Java tsunami, *Geophys. Res. Lett.,* **34,** L12602, doi:10.1029/2007GL029404.

Fritz, H.M., Kalligeris, N., Borrero, J.C., Broncano, P. & Ortega, E., 2008. The 15 August 2007 Peru tsunami runup observations and modeling, *Geophys. Res. Lett.,* **35,** L10604, doi:10.1029/2008GL033494.

Fritz, H.M. *et al*., 2011. Field survey of the 27 February 2010 Chile tsunami, *Pure appl. Geophys.,* **168,** 1989–2010, doi:10.1007/s00024-011-0283-5.

Fujii, Y. & Satake, K., 2006. Source of the July 2006 West Java tsunami estimated from tide gauge records, *Geophys. Res. Lett.,* **33,** L24317, doi:10.1029/2006GL028049.

Geist, E., Titov, V.V., Arcas, D., Pollitz, F.F. & Bilek, S.L., 2007. Implications of the 26 December 2004 Sumatra–Andaman earthquake on tsunami forecast and assessment models for great subduction-zone earthquakes, *Bull. seism. Soc. Am.,* **97**(1A), S249–S270, doi:10.1785/0120050619.

Hanka, W., Saul, J., Weber, B., Becker, J., Harjadi, P., Fauzi & GITEWS Seismology Group, 2010. Real-time earthquake monitoring for tsunami warning in the Indian Ocean and beyond, *Nat. Hazards Earth Syst. Sci.,* **10,** 2611–2622, doi:10.5194/nhess-10-2611-2010.

Hébert, H., Heinrich, P., Schindelé, F. & Piatanesi, A., 2001. Far-field simulation of tsunami propagation in the Pacific Ocean: impact on the Marquesas Islands (French Polynesia), *J. geophys. Res.,* **106,** 9161–9177.

Hébert, H., Sladen, A. & Schindelé, F., 2007. The great 2004 Indian Ocean tsunami: numerical modeling of the impact in the Mascarene Islands, *Bull. seism. Soc. Am.,* **97**(1A), S208–S222, doi:10.1785/0120050611.

Hébert, H., Reymond, D., Krien, Y., Vergoz, J., Schindelé, F., Roger, J. & Loevenbruck, A., 2009. The 15 August 2007 Peru earthquake and tsunami: influence of the source characteristics on the tsunami heights, *Pure appl. Geophys.,* **166,** 1–22.

Heinrich, P., Schindelé, F., Guibourg, S. & Ihmlé, P., 1998. Modeling of the February 1996 Peruvian tsunami, *Geophys. Res. Lett.,* **25,** 2687–2690.

Heinrich, P., Piatanesi, A. & Hébert, H., 2001. Numerical modelling of tsunami generation and propagation from submarine slumps: the 1998 Papua New Guinea event, *Geophys. J. Int.,* **145,** 97–111.

International Charter, 2011. International charter space and major disasters. Available at: http://www.disasterscharter.org/, last accessed 2011 June 17.

International Tsunami Information Center, 2006. Timeline: 17 July 2006, Java, Indonesia Earthquake and Tsunami, *ITIC Newsletters,* **XXXVIII**(3), 3–5.

IOC, IHO & BODC, 2003. *Centenary Edition of the GEBCO Digital Atlas,* British Oceanographic Data Centre, Liverpool. [Published on CD-ROM on behalf of the Intergovernmental Oceanographic Commission and the International Hydrographic Organization as part of the General Bathymetric Chart of the Oceans.]

Kanamori, H., 1972. Mechanism of tsunami earthquakes, *Phys. Earth planet. Inter.,* **6,** 346–359.

Kanamori, H. & Anderson, D., 1975. Theoretical basis of some empirical relations in seismology, *Bull. seism. Soc. Am.,* **65,** 1073–1095.

Kanamori, H. & Kikuchi, M., 1993. The 1992 Nicaragua earthquake: a slow tsunami earthquake associated with subducted sediments, *Nature,* **361,** 714–716.

Labbé, M., Donnadieu, C., Daubord, C. & Hébert, H., 2012. Refined numerical modeling of the 1979 tsunami in Nice (French Riviera): comparison with coastal data, *J. geophys. Res.,* **117,** F01008, doi:10.1029/2011JF001964.

Lavigne, F., Gomez, C., Giffo, M., Wassmer, P., Hoebeok, C., Mardiatno, D., Priyono, J. & Paris, R., 2007. Field survey and near field tsunami simulation, *Nat. Hazards Earth Syst. Sci.,* **7,** 177–183.

Maramai, S. & Tinti, S., 1997. The 3rd June, 1994 Java tsunami: a post-event survey of the coastal effects, *Nat. Hazards,* **15,** 31–49.

Moore, A. *et al*., 2011. Sedimentary deposits from the 17 July 2006 Western Java tsunami near Cilacap, Indonesia: use of grain size analyses to assess tsunami flow depth, speed, and traction carpet characteristics, *Pure appl. Geophys.,* **168,** 1951–9161, doi:10.1007/s00024-011-0280-8.

Mori, J., Mooney, W.D., Afnimar, Kurniawan, S., Anaya, A.I. & Widiyantoro, S., 2007. The 17 July 2006 tsunami earthquake in West Java, Indonesia, *Seism. Res. Lett.,* **78**(2), 201–207.

Okada, Y., 1985. Surface deformation due to shear and tensile faults in a halfspace, *Bull. seism. Soc. Am.,* **75,** 1135–1154.

Okal, E.A. & Synolakis, C.E., 2004. Source discriminants for near-field tsunamis, *Geophys. J. Int.,* **158,** 899–912, doi:10.1111/j.1365-246X.2004.02347.x.

Poisson, B., Oliveros, C. & Pedreros, R., 2011. Is there a best source model of the Sumatra 2004 earthquake for simulating the consecutive tsunami?, *Geophys. J. Int.,* **185,** 1365–1378.

Polet, J. & Kanamori, H., 2000. Shallow subduction earthquakes and their tsunamigenic potential, *Geophys. J. Int.,* **142,** 684–702.

Polet, J. & Thio, H.K., 2003. The 1994 Java tsunami earthquake and its "normal" aftershocks, *Geophys. Res. Lett.,* **30,** doi:10.1029/2002GL016806.

Satake, K., 1994. Mechanism of the 1992 Nicaragua tsunami earthquake, *Geophys. Res. Lett.,* **21,** 2519–2522.

Sladen, A. & Hébert, H., 2008. On the use of satellite altimetry to infer the earthquake rupture characteristics: application to the 2004 Sumatra event, *Geophys. J. Int.,* **172,** 707–714.

Yokota, Y., Koketsu, K., Fujii, Y., Satake, K., Sakai, S., Shinohara, M. & Kanazawa, T., 2011. Joint inversion of strong motion, teleseismic, geodetic, and tsunami datasets for the rupture process of the 2011 Tohoku earthquake, *Geophys. Res. Lett.,* **38,** L00G21, doi:10.1029/2011GL050098.